Arabian Journal of Chemistry (2021) **14**, 103032

King Saud University

Arabian Journal of Chemistry

www.ksu.edu.sa
www.sciencedirect.com

ORIGINAL ARTICLE

The effect of Mg concentration to mechanical strength of hydroxyapatite derived from eggshell

Atiek Rostika Noviyanti [a,*], **Iman Rahayu** [a], **Retna Putri Fauzia** [a], **Risdiana** [b]

[a] *Department of Chemistry, Universitas Padjadjaran, Jl. Raya Bandung-Sumedang km. 21 Jatinangor, Sumedang, West Jawa 45363 Indonesia*
[b] *Department of Physics, Universitas Padjadjaran, Jl. Raya Bandung-Sumedang km. 21 Jatinangor, Sumedang, West Jawa 45363 Indonesia*

Received 13 October 2020; accepted 19 January 2021
Available online 2 February 2021

KEYWORDS

Hydroxyapatite;
Hydrothermal;
Magnesium;
Whitlockite;
Vickers hardness

Abstract Hydroxyapatite (HA) of $Ca(I)_4Ca(II)_6(PO_4)_6(OH)_2$ is a biomaterial that is currently being developed for several biomedical applications, such as for the reconstruction of hard tissues of human bones and teeth. HA can be synthesized from raw materials that are easily found in large quantities in the world, such as eggshells. However, due to its low mechanical properties, the doping of metal ions of Mg in its structure is needed to improve the physical properties of HA. Five sets of HA-Mg composites with HA synthesized from eggshells and various MgO concentrations of 0.25, 0.50, 0.75, and 1.00 mol% were prepared by the hydrothermal method at 90 °C for 24 h to observe the effect of the amount of Mg doping on the structural, morphological, and mechanical properties of HA-Mg composites. Doping of Mg ion in HA has increased the secondary phase formation of whitlockite and enlarged the hardness value. The maximum hardness value of 88.7 HV was obtained from the highest Mg concentration of 1.00 mol%.

1. Introduction

Biomaterials are materials that are widely developed as basic materials for various medical applications because of their biocompatibility, bioactivity, and non-toxicity properties (Yazdani et al., 2018). Hydroxyapatite (HA) with the chemical formula $Ca(I)_4Ca(II)_6(PO_4)_6(OH)_2$ is a biomaterial that is currently being developed as a substitute for hard tissues, such as human bones and teeth in the field of orthopedics and dentistry (Wang et al., 2010). HA can assist in the integration process and new bone growth without disturbing the fibrous tissue progression (Rodríguez-Lugo et al., 2017). HA can be synthesized from raw materials that are easily found in large quantities in nature such as eggshells, limestone, coral, snail shells, and fish bones. For example, eggshells are found every day in several million tons as waste from the food industry or households and usually discarded without being processed, causing environmental problems during the biodegradation process. Eggshells constitute 11% of the total egg weight and mostly contain calcium in the form of $CaCO_3$ (Wu et al.,

* Corresponding author.
E-mail address: atiek.noviyanti@unpad.ac.id (A.R. Noviyanti).
Peer review under responsibility of King Saud University.

Production and hosting by Elsevier

https://doi.org/10.1016/j.arabjc.2021.103032

2016). Eggshell contains 94 to 97% $CaCO_3$ can be used as a good source of HA synthesis (Noviyanti et al., 2020).

HA has a unique chemical structure with two different Ca positions. Its unique structure allows the substitution of cations and anions to modify various properties of materials as well as to extend the functionality of HA in biomedical or other fields (Webster et al., 2004). The substitution of cations and anions in the HA structure is carried out by taking into account the size and electronegativity of the ion to be substituted in order to occupy and substitute Ca (I) or Ca (II). One of the properties of HA that limits the improvement of its function, especially in the medical field which needs to be modified is the mechanical properties of HA, namely the low strength of HA under applied compressive and tensile forces. For application needs in the biomedical field, HA must meet certain standard parameters, including good mechanical properties (Chakravarty et al., 2020). Structural modifications such as the substitution of cations or anions can be employed to increase the mechanical strength. Several studies have been reported that the morphology, stability, structure and mechanical properties of HA can be improved by doping metal ions (Gayathri et al., 2018). Metal ions that can be substituted into the HA structure are Zn (Li et al., 2008, Gross et al., 2013), Sr (Kaygili and Keser, 2015), Ag and Cu (Bostancioglu et al., 2017), Mn, Ni, Fe, Co (Robles-Águila et al., 2017) Ti (Jiraborvornpongsa et al., 2019), Mo (Jiraborvornpongsa et al., 2019), Te (Yahia et al., 2017), Se (Wu et al., 2020), and Ce (Priyadarshini et al., 2017).

The magnesium (Mg) ion is a metal ion that is essential for human metabolism and is naturally found in the bones and tissues of human teeth. Important cell osteogenic activity in calcium phosphate-based cement can be regulated by regulating the content of Mg ions in cement (Zhang et al., 2015). The magnesium ion is also very interesting to study as a metal ion that is substituted for HA. Based on ab initio simulations, the substitution of Mg to HA (Mg-HA) at a concentration of 25% Mg/Ca has increased the elastic properties of HA (Aryal et al., 2015). The mechanical properties and osteogenic activity of Mg-HA can be regulated by adjusting the Mg/Ca content to get good results when applying this Mg-HA material as a bone repair material (Li et al., 2020). Magnesium is also known to not only improve the mechanical properties of HA but also reduce the sintering temperature for densification (Montoya-Cisneros et al., 2017).

Apart from doping, mechanical properties can also be modified by applying appropriate synthesis methods to regulate morphological distribution, grain size and pore size. Several synthesis methods have been developed to produce HA, both pure HA and HA with metal ions doping, including using the precipitation method (Latocha et al., 2019, Tan et al., 2008), sol-gel method (Ben-Arfa et al., 2017, Gozaliana et al., 2011), hydrothermal (Noviyanti et al., 2020), wet chemical method (Stipniece et al., 2014), solid state reactions (Tardei et al., 2006), and microwave irradiation (Yedekçi et al., 2021). In our recent study (Noviyanti et al., 2020), HA was synthesized from chicken eggshells using a hydrothermal method at a lower temperature (90 °C) than previous studies (Wu et al., 2013, Li et al., 2020). This research has produced HA material with most of the promising mechanical properties due to its high purity and crystallinity.

Here we report the properties of HA doped with Mg synthesized by hydrothermal method to obtain HA-Mg material which has good mechanical properties for use in various medical purposes. HA is synthesized from chicken eggshells which are easily found in large quantities in Indonesia.

2. Experimental method

2.1. The synthesis of HA-Mg composites

The main part of HA, namely CaO powder, is synthesized from chicken eggshells by a simple process, as reported in our previous study (Noviyanti et al., 2020). This CaO powder was mixed with diammonium hydrogen phosphate with a Ca/P mole ratio of 1.67 then dissolved in a 0.2 M NaOH solution (pa Merck) which was added subsequently with MgO (pa EMSURE® Germany). Five sets of HA-Mg composites with various MgO concentrations of 0.25, 0.5, 0.75, and 1.00 mol % were prepared to observe the effect of the amount of Mg doping on the structural, morphological, and mechanical properties of HA-Mg composites. All HA-Mg composites were then named HA-Mg0.25, HA-Mg0.50, HA-Mg0.75, and HA-Mg1.00 for MgO concentrations of 0.25, 0.50, 0.75, and 1.00 mol%, respectively. For comparison, the synthesized HA without the addition of Mg is called HA. All HA-Mg composite sets were then synthesized by hydrothermal method by heating at 90 °C for 24 h.

2.2. The characterization of structure, morphology, and mechanical strength of HA-Mg composites

The entire synthesized HA-Mg was washed with DM water to neutral pH, dried at 100 °C for 1 h to remove water, and then sintered at 1000 °C for 5 h. The structure, morphology, and physical properties of all samples were characterized by XRD (Rigaku), FTIR (PerkinElmer Spectrum 100), and SEM-EDX (JEOL JSM-IT100 SEM), respectively. The grain size in all samples was analyzed using ImageJ software. The concentrations of Ca and Mg of the final samples were determined using energy dispersive X-ray spectroscopy (EDS).

The mechanical strength of Mg-HA was carried out by hardness testing on pellet samples that had been pressed and sintered at a temperature of 1000 °C using a Vickers hardness (HV) machine (Acme Automatic Digital Micro Hardness Series, LECO).

3. Results and discussion

3.1. Structure and morphology of HA-Mg

XRD patterns of HA and all Mg-HA composites of HA-Mg0.25, HA-Mg0.50, HA-Mg0.75, and HA-Mg1.00 are shown in Fig. 1.

All main peaks of HA with hexagonal structure and the space group of P_{63}/m are observed. The characteristic peaks of apatite phase are shown at 2θ of 25.7°, 31.7°, 33.0°, and 39.7° as matched with standard JCPDS file number of 9-0432. Impurity peaks of $C_3O_8P_2$ was observed in HA samples. For all HA-Mg composite samples, the secondary phase of Whitlockite, with the molecular formula of $Ca_{18}Mg_2H_2(PO_4)_{14}$ and hexagonal structure with the space group of R_3c are also discovered. The main peaks of HA are shifted slightly in

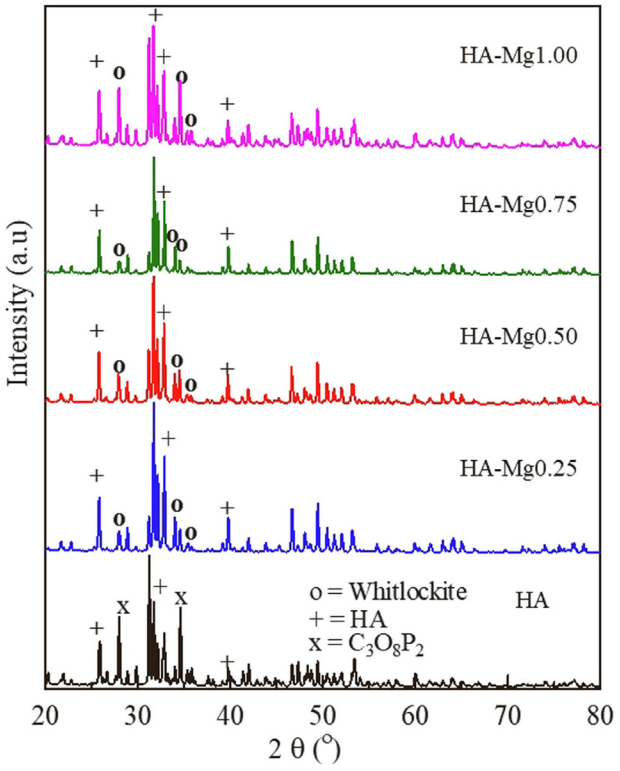

Fig. 1 XRD pattern of HA and HA-Mg0.25, HA-Mg0.50, HA-Mg0.75, and HA-Mg1.00.

HA-Mg samples to be 26°, 32°, 34° and 40° (Kanasan et al., 2018). The shift of the main peaks of HA due to the Mg content in the HA-Mg sample causes a slight contraction in the a-axis dimensions. Similar results were also reported in previous studies (Stipniece et al., 2014). The main peaks of whitlockite are located at 2θ in between 31° and 40° (Guo et al., 2018). The formation of whitlockite as a secondary phase appears to be due to the presence of magnesium, as also reported in previous studies (Trinkunaite-Felsen et al., 2014). The presence of two phases in HA-Mg composites, namely the HA phase and the whitlockite phase, is not actually a disadvantage because the appearance of these two phases allows an increased benefit of the material for biomedical applications. It is because materials with HA and whitlockite phases are reported to have excellent biocompatibility and show the increased ability for osteogenesis and mineralization (Hodge et al., 1938, Guo et al., 2018). It is already known that materials with whitlockite phase are harmless to the human body, proven to have been widely used in the field of pathology, especially in dental calculus and has an crucial influence on the development of hard tissue (Jang et al., 2015). The percentage contents of whitlockite phase of HA-Mg samples are shown in Table 1 (Trinkunaite-Felsen et al., 2014). The highest content of whitlockite phase is found in HA-Mg1.00. The low percentage content of whitlockite phase in HA-Mg0.75 is probably due low surface homogeneity. Synthesis temperature and presence of Mg ion are known to trigger the formation of whitlockite simultaneously in the formation of HA.

The shift of the HA peak to the higher angle occurs owing to differences in atomic size between Mg^{2+} ions and Ca^{2+} ions, where Mg^{2+} ions have smaller ionic radii of 0.72 Å compared to Ca^{2+} of 1.00 Å, which allows Mg ions to enter the HA structure (Chen et al., 2018). The change in lattice parameters in the *a*/*b* plane is slightly larger than that in the *c* plane, which strengthening the substitution of Mg ions in Ca ions located in the *a*/*b* plane. Mg doping in HA may result in the formation of shorter Mg–O bonds as explained in the previous research (Aryal et al., 2015). When defects and disorders occurred in the crystal structure of HA, the ratio of the major and minor axis changed, the crystallinity and grain size reduced. The crystallinity of synthesizing HA was calculated from the XRD data using the following equation Eq. (1) (Pal et al., 2017).

Table 1 Content of whitlockite in various HA-Mg.

Samples	Whitlockite/%
HA	00.0
HA-Mg0.25	22.0
HA-Mg0.50	35.3
HA-Mg0.75	18.8
HA-Mg1.00	53.2

$$X_c = 100 \times \left(I_{300} - V_{112/300}\right)/I_{300} \quad (1)$$

where I_{300} is the intensity of the diffraction peak at the (300), $V_{112/300}$ is the intensity of the (112) and (300), respectively. The crystallite size of Mg-HA nanoparticle is estimated by Scherrer's formula. The lattice parameter, crystal size, and crystallinity of HA and HA-Mg listed in Table 2.

Fig. 2 shows the FTIR results of HA and HA-Mg composites. It is found that the addition of the Mg dopant does not significantly change the appearance of the HA spectrum.

The presence of a slightly widened -PO_4 group is detected at 500–700 cm^{-1} due to the substitution of Mg ions, as mentioned in previous studies (Ben Moussa et al., 2018). In HA-Mg, the -PO_4 group appears at around 1200 cm^{-1} originated from the vibration of the secondary phase whitlockite (Suchanek et al., 2004). The higher the concentration of Mg ions added, the band change at the peaks in 945, 974, 988, 1117 and 1152 cm^{-1} increases (Stipniece et al., 2014). However, because the concentration of Mg is much smaller than 10%, it is difficult to observe the shifts in wave numbers and changes in band intensity. The peaks for whitlockite are in the range of 917 and 870 cm^{-1} as P-OH bond in HPO_4^{2-}, which is present in the structure, as also mentioned in the previous literature (Wang et al., 2020). The typical O-H cluster can be seen in 3500–3700 cm^{-1}. Meanwhile, the characteristic twin band of Mg-O is also observed at 1450 cm^{-1} from all HA-Mg samples (Noviyanti et al., 2020). The presence of the Mg-O band in HA can be explained because HA is synthesized from eggshells which naturally contain Mg even though in very small amounts.

The morphology of HA-Mg composites has been examined through SEM analysis, as seen in Fig. 3. It is found that the grain size of HA-Mg composites escalated with increasing Mg contents. The agglomeration occurred progressively as an increase of Mg in the composite indicated that the Mg dopant may improve the mechanical structure of the HA

Table 2 Lattice parameters of HA and HA-Mg.

Lattice Parameter			Crystal size (nm)	Crystallinity/%
Sample	$a = b$/Å	c/Å		
HA	9.4220(1)	6.879(1)	62.32	93.25
HA-Mg0.25	9.4148(1)	6.876(1)	62.41	92.68
HA-Mg0.50	9.4162(2)	6.866(1)	71.69	93.60
HA-Mg0.75	9.4166(1)	6.854(1)	80.49	90.16
HA-Mg1.00	9.4166(1)	6.851(1)	62.93	93.25

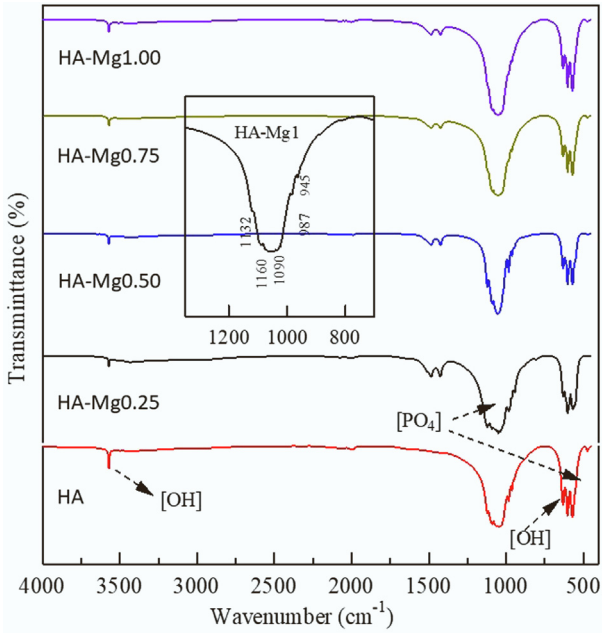

Fig. 2 IR Spectrum of HA, HA-Mg0.25, HA-Mg0.50, HA-Mg0.75, and HA-Mg1.00.

and HA-Mg composites. This behaviour complies with the crystal size of samples as listed in Table 2. The grain size in all samples was also analyzed using *ImageJ* software. It is found that the particle diameter increased slightly with increasing Mg concentration as shown in Table 3.

The shape of HA also changed with the Mg-substitution. The shape of HA grains looks like a cube and relatively homogeneous, while the morphology of HA-Mg formed agglomerates with the shape and size are not homogeneous. The grain shape appears to transform from round to slightly elliptical, while the grain boundaries tend to be stretched, corresponding to the crystal lattice alteration which tends to extend only in the a/b plane. Changes in the shape of HA particles are also very possible due to differences in whitlockite phase content in each sample, as mentioned in the previous report (Jang et al., 2015).

From EDS characterization, the Ca/P ratios of HA, HA-Mg 0.25, HA-Mg0.5, HA-Mg0.75, and HA-Mg1.00 are found to be 1.67, 1.65, 1.60, 1.57 and 1.76, respectively. The actual value of Ca/P ratio of HA-Mg0.75 was the smallest compared to other HA-Mg composites. This is probably related to the smallest percentage of crystallinity shown in Table 2.

3.2. The mechanical properties of HA-Mg

The mechanical properties of HA-Mg were examined in terms of the hardness (Vickers hardness/HV). Hardness is one of the essential parameters for comparing material properties. For this material, hardness tests are carried out to find the suitability of the clinical use of biomaterials (Roop Kumar and Wang, 2002). Mg ions can improve the mechanical properties of HA (Lala et al., 2017). The relationship of the hardness value with the concentration of Mg doping ion on HA is shown in Fig. 4. The higher the Mg doping concentration, the higher the value of HA-Mg hardness. This behaviour is in accordance with our findings in the morphology of HA-Mg composites. The addition of Mg ions to HA changes both the grain shape and the pore shape with the higher the Mg ion content the rounder the pore. This is thought to strongly influence the improvement of the mechanical properties of HA-Mg, as shown in previous studies (Veljović et al., 2011). The addition of magnesium with a concentration of 1.00 mol% can improve the hardness of HA up to 88.7 HV. The hardness of HA was doubled by adding 1.00 mol% of Mg to HA. The trend of HA values will continue to increase with the addition of Mg.

4. Conclusion

HA-Mg composites with CaO powder prepared from chicken eggshells are successfully synthesized by a hydrothermal method at 90 °C for 24 h in order to study effect of Mg ion substitution to HA on their structure, morphology, and hardness. The concentrations of Mg are 0.25, 0.50, 0.75 and 1.00 mol%. It is found that with increasing the Mg concentration, the content of the whitlockite phase increased. The grains tended to form ellipses and the grain size also escalated with increasing Mg content. The higher the Mg doping concentration, the higher the HA-Mg hardness value. The maximum hardness value of 88.7 HV was obtained from the highest Mg concentration of 1.00 mol%. This fact is verified by decreasing the lattice parameter a/b after Mg doping. It fits perfectly with the change in morphology of HA-Mg which becomes slightly to be more elliptical, with shorter grain boundaries. This alteration is possible, which is a strong reason for the increase in hardness in HA-Mg, apart from the nature of Mg and whitlockite content.

Declaration of Competing Interest

The authors declare that they have no known competing financial interests or personal relationships that could have appeared to influence the work reported in this paper.

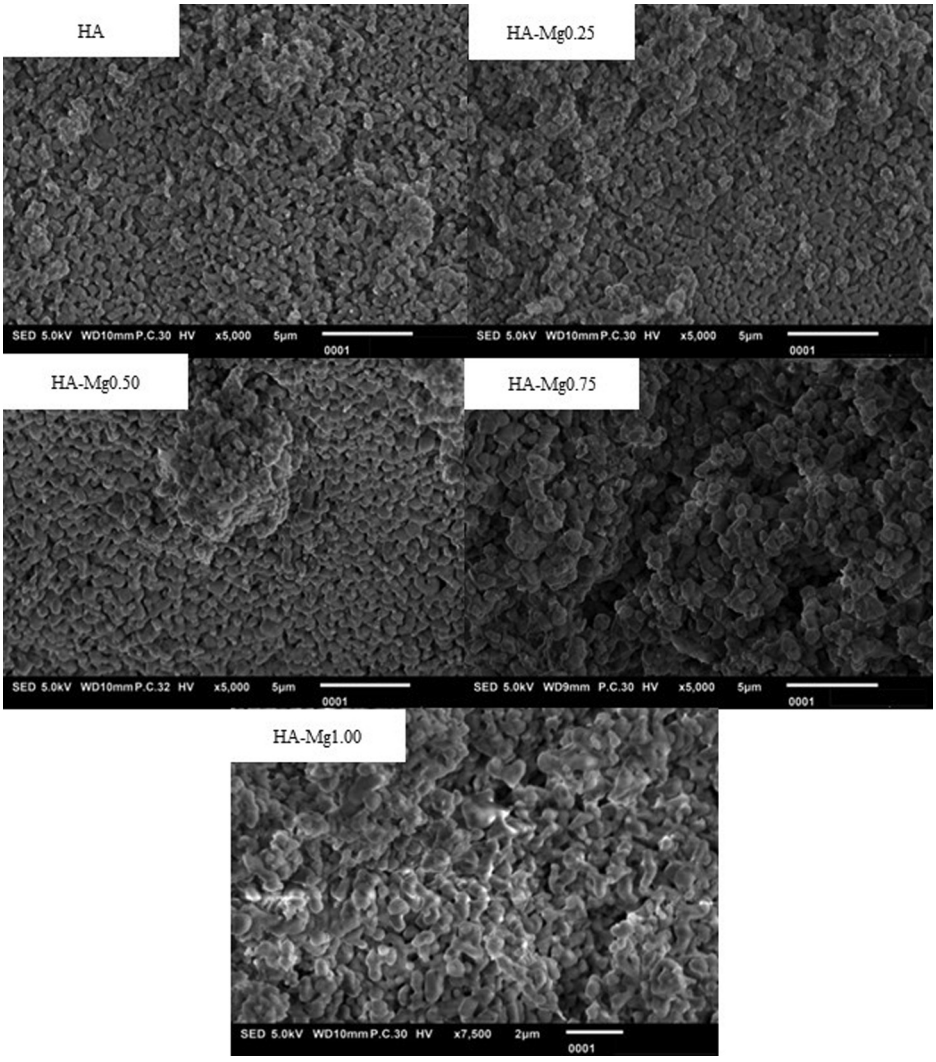

Fig. 3 The SEM micrograph of HA, HA-Mg 0.25, HA-Mg0.50, HA-Mg0.75, and HA-Mg1.00.

Table 3 The particle size diameter of HA-Mg composites.

Samples	Particle Diameter/μm
HA	0.69 ± 0.15
HA-Mg0.25	0.78 ± 0.11
HA-Mg0.50	0.91 ± 0.27
HA-Mg0.75	0.98 ± 0.26
HA-Mg1.00	1.06 ± 0.22

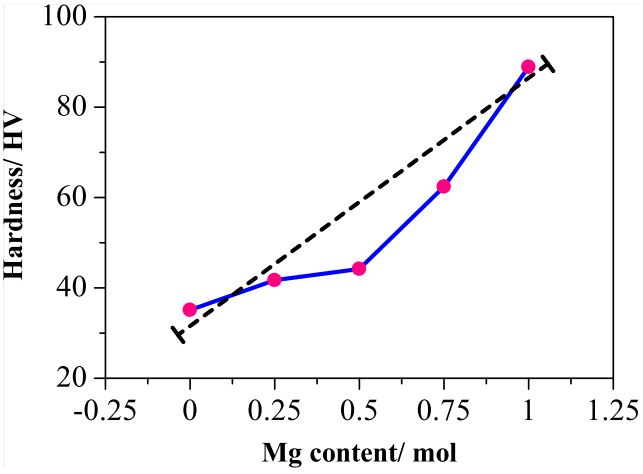

Fig. 4 Dependence of hardness to Mg content/mol of HA-Mg0.25, HA-Mg0.50, HA-Mg0.75, and HA-Mg1.00.

Acknowledgement

The authors would like to thank the Ministry of Research and Technology, Republic of Indonesia through PDUPT Research Grant No. 1827/UN6.3.1/LT/2020 and Academic Leadership Grant (ALG) No. 1427/UN6.3.1/LT/2020 for funding this research and to Elsyafahriza Risky for Preparing sample and Putri Rizka Lestari for supporting XRD measurement at Cen-

ter for Crystal Science and Technology, Graduate Faculty of Interdisciplinary Research, University of Yamanashi, Japan.

References

Aryal, S., Matsunaga, K., Ching, W.-Y., 2015. Ab initio simulation of elastic and mechanical properties of Zn- and Mg-doped hydroxyapatite (HAP). J. Mech. Behav. Biomed. Mater. 47, 135–146. https://doi.org/10.1016/j.jmbbm.2015.03.018.

Ben Moussa, S., Mehri, A., Gruselle, M., Beaunier, P., Costentin, G., Badraoui, B., 2018. Combined effect of magnesium and amino glutamic acid on the structure of hydroxyapatite prepared by hydrothermal method. Mater. Chem. Phys. 212, 21–29 https://doi.org/10.1016/j.matchemphys.2018.03.017.

Ben-Arfa, B.A.E., Salvado, I.M.M., Ferreira, J.M.F., Pullar, R.C., 2017. Novel route for rapid sol-gel synthesis of hydroxyapatite, avoiding ageing and using fast drying with a 50-fold to 200-fold reduction in process time. Mater. Sci. Eng. C 70, 796–804. https://doi.org/10.1016/j.msec.2016.09.054.

Bostancioglu, R.B., Gurbuz, M., Akyurekli, A.G., Dogan, A., Koparal, A.S., Koparal, A.T., 2017. Adhesion profile and differentiation capacity of human adipose tissue derived mesenchymal stem cells grown on metal ion (Zn, Ag and Cu) doped hydroxyapatite nano-coated surfaces. Colloids Surfaces B Biointerfaces 155, 415–428. https://doi.org/10.1016/j.colsurfb.2017.04.015.

Chakravarty, J., Rabbi, M.F., Chalivendra, V., Ferreira, T., Brigham, C.J., 2020. Mechanical and biological properties of chitin/polylactide (PLA)/hydroxyapatite (HAP) composites cast using ionic liquid solutions. Int. J. Biol. Macromol. 151, 1213–1223. https://doi.org/10.1016/j.ijbiomac.2019.10.168.

Chen, L., Chen, T., Cao, J., Liu, B., Shao, C., Zhou, K., Zhang, D., 2018. Effect of Tb/Mg doping on composition and physical properties of hydroxyapatite nanoparticles for gene vector application. Trans. Nonferrous Met. Soc. China 28, 125–136. https://doi.org/10.1016/S1003-6326(18)64645-X.

Gayathri, B., Muthukumarasamy, N., Velauthapillai, D., Santhosh, S. B., Asokan, V., 2018. Magnesium incorporated hydroxyapatite nanoparticles: Preparation, characterization, antibacterial and larvicidal activity. Arab. J. Chem. 11, 645–654. https://doi.org/10.1016/j.arabjc.2016.05.010.

Gozalian, A., Behnamghader, A., Daliri, M., Moshkforoush, A., 2011. Synthesis and thermal behavior of Mg-doped calcium phosphate nanopowders via the sol gel method. Sci. Iran. F 18, 1614–1622.

Gross, K.A., Komarovska, L., Viksna, A., 2013. Efficient zinc incorporation into hydroxyapatite through crystallization of an amorphous phase could extend the properties of zinc apatites. J. Aust. Ceram. Soc. 49, 129–135.

Guo, X., Liu, X., Gao, H., Shi, X., Zhao, N., Wang, Y., 2018. Hydrothermal growth of whitlockite coating on β-tricalcium phosphate surfaces for enhancing bone repair potential. J. Mater. Sci. Technol. 34, 1054–1059. https://doi.org/10.1016/j.jmst.2017.07.009.

Hodge, H.C., LeFevre, M.L., Bale, W.F., 1938. Chemical and X-ray diffraction studies of calcium phosphates. Ind. Eng. Chem. Anal. 10, 156–161.

Jang, H.L., Lee, H.K., Jin, K., Ahn, H.-Y., Lee, H.-E., Nam, K.T., 2015. Phase transformation from hydroxyapatite to the secondary bone mineral, whitlockite. J. Mater. Chem. B 3, 1342–13493.

Jiraborvornpongsa, N., Isobe, T., Matsushita, S., Oshikiri, M., Wakamura, M., Fujii, K., Yashima, M., Nakajima, A., 2019. Preparation and photocatalytic activity of Mo-modified Ti-doped HAp. Appl. Catal. B Environ. 243, 448–454. https://doi.org/10.1016/j.apcatb.2018.10.056.

Kanasan, N., Adzila, S., Rahman, H.A., Bano, N., Panerselvan, G., Hidayati, N.A., 2018. FTIR and XRD evaluation of magnesium doped hydroxyapatite/sodium alginate powder by precipitation method. Key Eng. Mater. 791, 45–49. https://doi.org/10.4028/www.scientific.net/kem.791.45.

Kaygili, O., Keser, S., 2015. Sol–gel synthesis and characterization of Sr/Mg, Mg/Zn and Sr/Zn co-doped hydroxyapatites. Mater. Lett. 141, 161–164. https://doi.org/10.1016/j.matlet.2014.11.078.

Lala, S., Maity, T.N., Singha, M., Biswas, K., Pradhan, S.K., 2017. Effect of doping (Mg, Mn, Zn) on the microstructure and mechanical properties of spark plasma sintered hydroxyapatites synthesized by mechanical alloying. Ceram. Int. 43, 2389–2397. https://doi.org/10.1016/j.ceramint.2016.11.027.

Latocha, J., Wojasiński, M., Sobieszuk, P., Gierlotka, S., Ciach, T., 2019. Impact of morphology-influencing factors in lecithin-based hydroxyapatite precipitation. Ceram. Int. 45, 21220–21227. https://doi.org/10.1016/j.ceramint.2019.07.103.

Li, M., Xiao, X., Liu, R., Chen, C., Huang, L., 2008. Structural characterization of zinc-substituted hydroxyapatite prepared by hydrothermal method. J. Mater. Sci. Mater. Med. 19, 797–803.

Li, W., Lu, Y., Liu, K., Wen, W., Liu, M., Li, H., Zhou, C., Luo, B., 2020. Preparation of HAp whiskers with or without Mg ions and their effects on the mechanical properties and osteogenic activity of poly(d, l-lactide). Compos. Part B Eng. 196,. https://doi.org/10.1016/j.compositesb.2020.108137 108137.

Montoya-Cisneros, K.L., Rendón-Angeles, J.C., Matamoros-Veloza, Z., Matamoros-Veloza, A., Yanagisawa, K., 2017. Low-temperature densification of Mg-doped hydroxyapatite fine powders under hydrothermal hot processing conditions. Ceram. Int. 43, 11907–11919. https://doi.org/10.1016/j.ceramint.2017.06.039.

Noviyanti, A.R., Akbar, N., Deawati, Y., Engela Evy Ernawati, Y.T. M., Retna Putri Fauzia, R., 2020. A novel hydrothermal synthesis of nanohydroxyapatite from eggshell-calcium-oxide precursors. Heliyon 6, e03655.

Pal, A., Paul, S., Choudhury, A.R., Balla, V.K., Das, M., Sinha, A., 2017. Synthesis of hydroxyapatite from Lates calcarifer fish bone for biomedical applications. Mater. Lett. 203, 89–92. https://doi.org/10.1016/j.matlet.2017.05.103.

Priyadarshini, B., Anjaneyulu, U., Vijayalakshmi, U., 2017. Preparation and characterization of sol-gel derived Ce^{4+} doped hydroxyapatite and its in vitro biological evaluations for orthopedic applications. Mater. Des. 119, 446–455. https://doi.org/10.1016/j.matdes.2017.01.095.

Robles-Águila, M.J., Reyes-Avendaño, J.A., Mendoza, M.E., 2017. Structural analysis of metal-doped (Mn, Fe Co, Ni, Cu, Zn) calcium hydroxyapatite synthetized by a sol-gel microwave-assisted method. Ceram. Int. 43, 12705–12709. https://doi.org/10.1016/j.ceramint.2017.06.154.

Rodríguez-Lugo, V., Salinas-Rodríguez, E., Vázquez, R.A., Alemán, K., Rivera, A.L., 2017. Hydroxyapatite synthesis from a starfish and β-tricalcium phosphate using a hydrothermal method. RSC Adv. 7, 7631–7639. https://doi.org/10.1039/c6ra26907a.

Roop Kumar, R., Wang, M., 2002. Modulus and hardness evaluations of sintered bioceramic powders and functionally graded bioactive composites by nano-indentation technique. Mater. Sci. Eng. A 338, 230–236. https://doi.org/10.1016/S0921-5093(02)00080-1.

Stipniece, L., Salma-Ancane, K., Borodajenko, N., Sokolova, M., Jakovlevs, D., Berzina-Cimdina, L., 2014. Characterization of Mg-substituted hydroxyapatite synthesized by wet chemical method. Ceram. Int. 40, 3261–3267. https://doi.org/10.1016/j.ceramint.2013.09.110.

Suchanek, W.L., Byrappa, K., Shuk, P., Riman, R.E., Janas, V.F., TenHuisen, K.S., 2004. Mechanochemical-hydrothermal synthesis of calcium phosphate powders with coupled magnesium and carbonate substitution. J. Solid State Chem. 177, 793–799. https://doi.org/10.1016/j.jssc.2003.09.012.

Tan, C.Y., Aw, K.L., Yeo, W.H., Ramesh, S., Hamdi, M., Sopyan, I., 2008. Influence of magnesium doping in hydroxyapatite ceramics. Biomed 21, 326–329.

Tardei, C., Grigor, F., Pasuk, I., Stoleri, S., 2006. The study of Mg^{2+} / Ca^{2+} substitution of -tricalcium phosphat. J. Optoelectron. Adv. Mater. 8, 568–571.

Trinkunaite-Felsen, J., Stankeviciute, Z., Yang, J.C., Yang, T.C.K., Beganskiene, A., Kareiva, A., 2014. Calcium hydroxyapatite/whitlockite obtained from dairy products: Simple, environmentally benign and green preparation technology. Ceram. Int. 40, 12717–12722. https://doi.org/10.1016/j.ceramint.2014.04.120.

Veljović, D., Jančić-Hajneman, R., Balać, I., Jokić, B., Putić, S., Petrović, R., Janaćković, D., 2011. The effect of the shape and size of the pores on the mechanical properties of porous HAP-based bioceramics. Ceram. Int. 37, 471–479. https://doi.org/10.1016/j.ceramint.2010.09.014.

Wang, C., Jeong, K.-J., Park, H.J., Lee, M., Ryu, S.-C., Hwang, D.Y., Nam, K.H., Han, I.H., Lee, J., 2020. Synthesis and formation mechanism of bone mineral, whitlockite nanocrystals in tri-solvent system. J. Colloid Interface Sci. 569, 1–11. https://doi.org/10.1016/j.jcis.2020.02.072.

Wang, P., Li, C., Gong, H., Jiang, X., Wang, H., Li, K., 2010. Effects of synthesis conditions on the morphology of hydroxyapatite nanoparticles produced by wet chemical process. Powder Technol. 203, 315–321. https://doi.org/10.1016/j.powtec.2010.05.023.

Webster, T.J., Massa-Schlueter, E.A., Smith, J.L., Slamovich, E.B., 2004. Osteoblast response to hydroxyapatite doped with divalent and trivalent cations. Biomaterials 25, 2111–2121. https://doi.org/10.1016/j.biomaterials.2003.09.001.

Wu, S.-C., Hsu, H.-C., Hsu, S.-K., Chang, Y.-C., Ho, W.-F., 2016. Synthesis of hydroxyapatite from eggshell powders through ball milling and heat treatment. J. Asian Ceram. Soc. 4, 85–90. https://doi.org/10.1016/j.jascer.2015.12.002.

Wu, S.C., Tsou, H.K., Hsu, H.C., Hsu, S.K., Liou, S.P., Ho, W.F., 2013. A hydrothermal synthesis of eggshell and fruit waste extract to produce nanosized hydroxyapatite. Ceram. Int. 39, 8183–8188. https://doi.org/10.1016/j.ceramint.2013.03.094.

Wu, V.M., Ahmed, M.K., Mostafa, M.S., Uskoković, V., 2020. Empirical and theoretical insights into the structural effects of selenite doping in hydroxyapatite and the ensuing inhibition of osteoclasts. Mater. Sci. Eng. C 117,. https://doi.org/10.1016/j.msec.2020.111257 111257.

Yahia, I.S., Shkir, M., AlFaify, S., Ganesh, V., Zahran, H.Y., Kilany, M., 2017. Facile microwave-assisted synthesis of Te-doped hydroxyapatite nanorods and nanosheets and their characterizations for bone cement applications. Mater. Sci. Eng. C 72, 472–480. https://doi.org/10.1016/j.msec.2016.11.074.

Yazdani, J., Ahmadian, E., Sharifi, S., Shahi, S., Maleki Dizaj, S., 2018. A short view on nanohydroxyapatite as coating of dental implants. Biomed. Pharmacother. 105, 553–557. https://doi.org/10.1016/j.biopha.2018.06.013.

Yedekçi, B., Tezcaner, A., Alshemary, A.Z., Yılmaz, B., Demir, T., Evis, Z., 2021. Synthesis and sintering of B, Sr, Mg multi-doped hydroxyapatites: Structural, mechanical and biological characterization. J. Mech. Behav. Biomed. Mater. 115,. https://doi.org/10.1016/j.jmbbm.2020.104230 104230.

Zhang, J., Ma, X., Lin, D., Shi, H., Yuan, Y., Tang, W., Zhou, H., Guo, H., Qian, J., Liu, C., 2015. Magnesium modification of a calcium phosphate cement alters bone marrow stromal cell behavior via an integrin-mediated mechanism. Biomaterials 53, 251–264. https://doi.org/10.1016/j.biomaterials.2015.02.097.